Eliott	Guenat	Eliott.guenat@epfl.ch
First	*Last*	*E-mail*

Paper title Effects of humid air on aerodynamic journal bearings

Authors: Guenat, Eliott ; Schiffmann, Jürg

Elsevier journal Tribology International

Transactions: Volume 127, Pages 333-340

Date of Publication: 15.06.2018

DOI: https://doi.org/10.1016/j.triboint.2018.06.002

Science direct https://www.sciencedirect.com/science/article/pii/S0301679X18302883?via%3Dihub

Effects of humid air on aerodynamic journal bearings

Eliott Guenat[1], Jürg Schiffmann

Ecole Polytechnique Fédérale de Lausanne, Laboratory for applied mechanical design, Maladière 71b, CP 526, CH-2002 Neuchâtel 2

Abstract

The development of aerodynamic bearings applications where ambient conditions cannot be controlled (e.g., for automotive fuel cell compressor) raises the question of the effects of condensation in the humid air on performance. A modified Reynolds equation is obtained in relation to humid air thermodynamic equations, accounting for the variation of compressibility and viscosity in the gas mixture. The load capacity and stability of plain and herringbone-grooved journal bearings is computed on a wide range of operating and ambient conditions. In general, performance metrics show an independence on humid-air effects at moderated temperature, although the stability of the grooved journal bearing exhibits strong variations in particular conditions. In consequence, a safety margin of 25% is suggested for the critical mass.

Keywords: Aerodynamic Lubrication, Gas Bearings, Humid air, Simulation

[1]Corresponding author. Email adress: eliott.guenat@epfl.ch

a	Groove length (m)
b	Ridge length (m)
C	Damping (N s m^{-1})
c_s	NGT coefficient (-)
c	Viscosity coefficient (-)
$\tilde{c}$	Molar concentration (-)
D	Bearing diameter (m)
e	Eccentricity (m)
f	NGT coefficient (-)
g	NGT coefficient (-)
H	Groove depth ratio h_g/h_0 at $\epsilon = 0$ (-)
h	Clearance (m)
h_0	Nominal clearance (m)
h_g	Groove clearance (m)
h_r	Ridge clearance (m)
K	Stiffness (N m$^-1$)
L	Bearing length (m)
M_c	Critical mass (kg)
M_r	Critical mass ratio (-)
$\tilde{m}$	Molar mass (kg mol^{-1})
P	Pressure (Pa)
R	Radius (m)
r	Specific gas constant (J kg^{-1}K^{-1})
T	Temperature (K)
t	Time (s)
U	Bearing tangential velocity (m/s)
W	Load capacity (N)
W_r	Load capacity ratio (-)
w	Humidity ratio (-)
X	Coordinate in the direction of the displacement (m)
x	Coordinate in the inertial frame (m)
y	Coordinate in the inertial frame (m)
z	Axial coordinate (m)
	Greek symbols
α	Groove aspect ratio (-)
β	Bulk modulus (Pa)
$\hat{\beta}$	Groove angle (rad)

ϵ	Eccentricity ratio (-)
θ	Circumferential coordinate (rad)
Λ	Compressibility number (-)
μ	Dynamic viscosity (Pa s)
ρ	Density (kg m^{-3})
σ	Squeeze number (-)
Φ	Viscosity coefficient (-)
ϕ	Relative humidity (-)
Ω	Bearing angular velocity (rad s^{-1})
ω	Excitation angular velocity (rad s^{-1})
	Superscripts
$-$	Normalized
$*$	Saturated
	Subscripts
a	Ambient condition
air	Air
c	Critical
$cond$	Condensable
g	Groove
$non-cond$	Non-condensable
r	Ridge, ratio
T	Isothermal
vap	Water vapor (gas phase)
w	Water liquid phase
x	x-axis
y	y-axis
z	z-axis
0	Static, unperturbed
1	Perturbed
	Acronyms
HA	Humid air
$HGJB$	Herringbone grooved journal bearing
PJB	Plain journal bearing
NGT	Narrow groove theory

1. Introduction

The use of aerodynamic bearings expands progressively to domains where the ambient conditions cannot be satisfactorily conditioned, either due to economical or to technical reasons. In particular, gas bearing-supported pressurizers of Proton-Exchange Membrane (PEM) fuel cells [1, 2, 3] for automotive applications are subject to a large range of ambient temperatures and relative humidities. Thus, the knowledge of the effect of ambient humidity on the performance of an aerodynamic bearing is necessary to ensure the viability of a given design.

1.1. Nature of the issue

Water vapor contained in humid air (HA) is subject to condensation if the saturation pressure is reached within the fluid film of gas-lubricated bearings. The resulting effects might influence the bearing behavior. Several works [4, 5] theoretically and experimentally investigated the influence of HA on the static pressure field of hard disk drive heads, showing that vapor condensation can occur, which reduces the pressure in the bearing, leading to a reduction of the head's flying height. For the same application, Hua et al. [6] performed transient simulations investigating the settling time of the flying head and showed that HA effects affect the final state of the bearing. In the previously mentioned works, the simulation method to model HA effects consists in applying a correction on the pressure field obtained from the ideal-gas form of the Reynolds equation. Kirpekar et al. [7] introduced a modification of the Reynolds equation to obtain a more rigorous approach. Ma et Liu [8, 9] investigated the dynamic phase equilibrium in the mixture to conclude to the quasi-immediacy of the thermodynamic equilibrium in the gas film. Aoki et al. [10] experimentally highlighted the influence of the water film thickness on the behavior of the bearing in ultra-thin film lubrication. More recently, the same phenomenon was further studied by Choi et al. [11]. Tani et al.[12] measured the clearance loss in a slider bearing lubricated with with water-nitrogen and ethanol-nitrogen mixtures and further confirmed the clearance reduction in humid conditions. Ma et al. [13] theoretically studied the influence of the adsorbed water film on the heat transfer in a slider bearing, highlighting an increase of the heat transfer coefficient. Matthes et al. [14, 15] experimentally investigated the influence of relative humidity on the touch-down power of an aerodynamic slider bearing. They reported a reduction of touch-down energy loss with increasing humidity ratios. The literature on the HA-lubricated bearings is still limited to slider geometries with ultra-thin film lubrication applied to data storage, with no application to journal bearings, despite the growing interest for aerodynamic bearings employed in humid environments.

1.2. Goals and objectives

The present work investigates the HA effects on the performance of plain journal bearings (PJB) and of herringbone-grooved journal bearings (HGJB). The objectives are to: (1) develop an expression of the Reynolds equation for HA-lubricated journal bearings, (2) evaluate the deviation of HA-lubricated journal bearing from ideal-gas lubrication in terms of load capacity and whirl stability in a large range of ambient temperatures, relative humidities and operating conditions and (3) devise design guidelines for robust design considering HA effects.

1.3. Scope of the Paper

The Reynolds equation for compressible fluids is adapted to express the local density, exhibiting the bulk modulus whose expression depends on whether the saturation conditions are locally met or not. The expression of the bulk modulus is derived from the classical humid air theory and accounts for the drying effect of condensing vapor. The perturbation method is applied on the Reynolds equation and a finite difference scheme is used to solve the equations. Static and dynamic bearing properties are obtained by integration of the pressure fields. The concept of critical mass is used as a stability metric regarding the whirl instability. The deviation of HA lubrication from the ideal-gas case is investigated for both PJB and HGJB in terms of load capacity and critical mass. The selected HGJB geometry maximizes the stability at moderated compressibility number ($\Lambda = 1$). The considered operating conditions vary in temperature from 275 to 370 K, in relative humidity from 0 to 1 with different eccentricity ratios and compressibility numbers up to 30. Based on the generated results, a set of design guidelines is suggested for the design of HA-lubricated journal bearings based on the ideal-gas Reynolds equation.

2. Theory

HA lubrication implies a condensable gas mixture of water (condensable) and air, considered as incondensable. The main working hypotheses in the following development are as follows: (1) the gas film is isothermal, (2) the thermodynamic equilibrium is instantaneous as suggested by Ma et Liu [8], (3) only the gas phase is considered. The hypothesis (1) is justified by the large contact area of the gas film with the rotor and bushings. These areas are heterogeneous nucleation sites justifying (2) and the very small volume of condensed water regarding the gas phase justifies (3). The Reynolds equation adds the hypothesis of thin film, laminar flow, Newtonian fluid and negligible inertial effects. It is recalled as follows:

$$\partial_X \left(\frac{\rho h^3}{12\mu} \partial_X P \right) + \partial_z \left(\frac{\rho h^3}{12\mu} \partial_z P \right) = \frac{U}{2} \partial_X (\rho h) + \partial_t (\rho h) \tag{1}$$

Since the practical problem targeted in the present work involves an atmospheric pressure, both gases (air and water vapor) are considered as ideal. However, for an isothermal gas, the saturation partial pressure of water can be reached within the film as mixture pressure increases. At this point (dew point), water vapor starts condensing and limits its contribution to the mixture pressure build-up on which the bearing relies to serve its purpose. At this point, the behavior of the mixture deviates from an ideal gas, namely:

$$P = \rho r_a T \tag{2}$$

where r_a is the specific gas constant of the ambient HA. In order to account for the condensation effects, Equation 2 is not used to substitute the density with the pressure in Reynolds equation. Instead, the following changes of variable are applied:

$$\frac{\partial P}{\partial X} = \left(\frac{\partial P}{\partial \rho} \right)_T \cdot \frac{\partial \rho}{\partial X}, \qquad \frac{\partial P}{\partial z} = \left(\frac{\partial P}{\partial \rho} \right)_T \cdot \frac{\partial \rho}{\partial z} \tag{3}$$

Where $(\partial_\rho P)_T$ is associated to the bulk modulus β of the lubricant gas:

$$\rho \left(\frac{\partial P}{\partial \rho} \right)_T = \beta \tag{4}$$

The following normalization is performed on Equation 1 to express it in cylindrical coordinates (Equation 6):

$$\begin{aligned} \bar{\rho} = \rho/\rho_a \quad \bar{\mu} = \mu/\mu_a \quad \bar{\beta} = \beta/P_a \quad \theta = X/R \\ \bar{z} = z/R \quad \bar{h} = h/h_0 \quad \bar{t} = t\omega \end{aligned} \tag{5}$$

$$\partial_\theta \left(\frac{\bar{\beta}\bar{h}^3}{\bar{\mu}} \partial_\theta \bar{\rho} \right) + \partial_{\bar{z}} \left(\frac{\bar{\beta}\bar{h}^3}{\bar{\mu}} \partial_{\bar{z}} \bar{\rho} \right) = \Lambda \partial_\theta \left(\bar{\rho}\bar{h} \right) + \sigma \partial_{\bar{t}} \left(\bar{\rho}\bar{h} \right) \tag{6}$$

Where Λ and σ are the compressibility and squeeze number respectively, defined as follows for journal bearings (Figure A.1):

$$\Lambda = \frac{6\mu_a \Omega R^2}{P_a h_0^2} \tag{7}$$

$$\sigma = 2\Lambda \frac{\omega}{\Omega} \tag{8}$$

In order to obtain the dynamic coefficients and to compute the critical mass, the clearance is perturbed by an infinitesimal harmonic motion ϵ_{1x} and ϵ_{1y} ($\epsilon_{x/y} = e_{x/y}/h_0$) in the x and y directions respectively [16]:

$$\begin{aligned} \bar{h} =& \bar{h}_0 - \epsilon_{1x} \cos\theta e^{i\bar{t}} - \epsilon_{1y} \sin\theta e^{i\bar{t}} && (9) \\ =& 1 - \epsilon_{0x} \cos\theta - \epsilon_{0y} \sin\theta - \epsilon_{1x} \cos\theta e^{i\bar{t}} - \epsilon_{1y} \sin\theta e^{i\bar{t}} && (10) \end{aligned}$$

where ϵ_{0x} and ϵ_{0y} are the static equilibrium eccentricity ratios. The other perturbed terms involved in Equation 7 are:

$$\bar{\rho} = \bar{\rho}_0 + \epsilon_{1x}\bar{\rho}_{1x} e^{i\bar{t}} + \epsilon_{1y}\bar{\rho}_{1y} e^{i\bar{t}} \tag{11}$$

$$\bar{\beta} = \bar{\beta}_0 + \epsilon_{1x} \left(\frac{\partial \bar{\beta}}{\partial \bar{\rho}} \right)_0 \bar{\rho}_{1x} e^{i\bar{t}} + \epsilon_{1y} \left(\frac{\partial \bar{\beta}}{\partial \bar{\rho}} \right)_0 \bar{\rho}_{1y} e^{i\bar{t}} \tag{12}$$

$$\frac{1}{\bar{\mu}} = \frac{1}{\bar{\mu}_0} + \epsilon_{1x} \left(\frac{-1}{\bar{\mu}^2} \frac{\partial \bar{\mu}}{\partial \bar{\rho}} \right)_0 \bar{\rho}_{1x} e^{i\bar{t}} + \epsilon_{1y} \left(\frac{-1}{\bar{\mu}^2} \frac{\partial \bar{\mu}}{\partial \bar{\rho}} \right)_0 \bar{\rho}_{1y} e^{i\bar{t}} \tag{13}$$

Terms of order 0 and 1 with respect to ϵ_{1x} and ϵ_{1y} are retained and grouped in Equations 14 and 15 respectively. The same procedure is reiterated in the y direction without being repeated here.

$$\partial_\theta \left[\frac{\bar{\beta}_0 \bar{h}_0^3}{\bar{\mu}_0} \partial_\theta \bar{\rho}_0 \right] + \partial_{\bar{z}} \left[\frac{\bar{\beta}_0 \bar{h}_0^3}{\bar{\mu}_0} \partial_{\bar{z}} \bar{\rho}_0 \right] - \Lambda \partial_\theta \left(\bar{\rho}_0 \bar{h}_0 \right) = 0 \tag{14}$$

$$
\begin{aligned}
&\partial_\theta \left[\left(\frac{\partial \bar{\beta}}{\partial \bar{\rho}} \right)_0 \bar{\rho}_{1x} \frac{\bar{h}_0^3}{\bar{\mu}_0} \partial_\theta \bar{\rho}_0 + \bar{\beta}_0 \left(\frac{-1}{\bar{\mu}^2} \frac{\partial \bar{\mu}}{\partial \bar{\rho}} \right)_0 \bar{\rho}_{1x} \bar{h}_0^3 \partial_\theta \bar{\rho}_0 + \right. \\
&\qquad \left. \frac{\bar{\beta} 3 \bar{h}_0^2}{\bar{\mu}_0} \cos\theta \partial_\theta \bar{\rho}_0 + \frac{\bar{\beta}_0 \bar{h}_0^3}{\bar{\mu}_0} \partial_\theta \bar{\rho}_{1x} \right] \\
&+ \partial_{\bar{z}} \left[\left(\frac{\partial \bar{\beta}}{\partial \bar{\rho}} \right)_0 \bar{\rho}_{1x} \frac{\bar{h}_0^3}{\bar{\mu}_0} \partial_\theta \bar{\rho}_0 + \bar{\beta}_0 \left(\frac{-1}{\bar{\mu}^2} \frac{\partial \bar{\mu}}{\partial \bar{\rho}} \right)_0 \bar{\rho}_{1x} \bar{h}_0^3 \partial_\theta \bar{\rho}_0 + \right. \\
&\qquad \left. \frac{\bar{\beta} 3 \bar{h}_0^2}{\bar{\mu}_0} \cos\theta \partial_\theta \bar{\rho}_0 + \frac{\bar{\beta}_0 \bar{h}_0^3}{\bar{\mu}_0} \partial_\theta \bar{\rho}_{1x} \right] \\
&- \Lambda \partial_\theta \left(\bar{\rho}_0 \cos\theta + \bar{\rho}_{1x} \bar{h}_0 \right) - i\sigma \left(\bar{\rho}_0 \cos\theta + \bar{\rho}_{1x} \bar{h}_0) \right) = 0
\end{aligned}
\tag{15}
$$

A central finite difference scheme is employed to discretize the equations with the boundary conditions of periodicity for $\theta = 0$ and $\theta = 2\pi$ and ambient density at $\bar{z} = \pm L/D$. The procedure consists in solving successively both unperturbed and perturbed equations to obtain the corresponding pressure fields, integrating them over the bearing domain to get the load capacity and complex impedances leading to the computation of the critical mass [17].

The same method can be applied to the HGJB using the Narrow Groove Theory (NGT) to obtain a modified Reynolds equation [18]. This procedure predicts the overall pressure generated by an infinite number of groove-ridge pairs over the bearing domain, smoothing the local pressure variation over a ridge-groove pair. Only the resulting differential equation is displayed here:

$$
\begin{aligned}
&\partial_\theta \left[\bar{\beta} \left(f_1 \partial_\theta \bar{\rho} + f_2 \partial_{\bar{z}} \bar{\rho} \right) \right] + \partial_{\bar{z}} \left[\bar{\beta} \left(f_2 \partial_\theta \bar{\rho} + f_3 \partial_{\bar{z}} \bar{\rho} \right) \right] \\
&\qquad + c_s \left(\sin\hat{\beta} \partial_\theta (f_4 \bar{\rho}) - \cos\hat{\beta} \partial_{\bar{z}} (f_4 \bar{\rho}) \right) \\
&\qquad - \Lambda \partial_\theta (f_5 \bar{\rho}) - \sigma \partial_{\bar{t}} (f_5 \bar{\rho}) = 0
\end{aligned}
\tag{16}
$$

where the geometry is presented in Figure A.2 and functions f_i are summarized in the Appendix. A first-order perturbation is applied to this equation following Equations 9 to 13 and zeroth- and first-order equations are segregated to be solved successively.

The problem of HA lubrication consists in the expression of $(\partial_{\bar{\rho}} \bar{P})_T$. As long as the saturation partial pressure of water vapor is not locally reached, the mixture is assumed to be an ideal gas. Thus, the term $(\partial_{\bar{\rho}} \bar{P})_T$, encapsulated in the bulk modulus, is equal to unity:

$$
(\partial_{\bar{\rho}} \bar{P})_T = \frac{\rho_a}{P_a} (\partial_\rho P)_T = \frac{\rho_a r_a T}{P_a} = 1 \tag{17}
$$

Only when the saturation pressure is met, condensing water will stop building up pressure, leading to $(\partial_{\bar{\rho}}\bar{P})_T < 1$, thus, departing from the ideal-gas behavior.

The ideal-gas equation for the gas mixture is:

$$P = \rho r T \tag{18}$$

The value of $(\partial_\rho P)_T$ is simply:

$$(\partial_\rho P)_T = rT + \rho T \partial_\rho r \tag{19}$$

where r is the mixture specific gas constant

$$r = \frac{r_{air} + w r_{vap}}{1 + w} \tag{20}$$

and w is the humidity ratio defined as the ratio of mass water vapor per unit mass of dry air:

$$w = \frac{M_{vap}}{M_{air}} \tag{21}$$

The value of w of the gas phase is defined locally depending on whether the saturation conditions are met or not:

$$w = \min(w_a, w^*(T_a, P)) \tag{22}$$

w^* is the saturation humidity ratio, which is a function of the ambient temperature and local pressure as follows:

$$w^* = \frac{\tilde{m}_{vap}}{\tilde{m}_{air}} \frac{P^*_{vap}(T_a)}{P - P^*_{vap}(T_a)} \tag{23}$$

where P^*_{vap} is the saturation pressure of water that depends on the temperature only, computed using a fluid database [19]. Since Equation 6 deals with density rather than pressure, it is convenient to have an expression of w^* as a function of density. For that purpose Equation 18 is inserted in Equation 23 and w^* is isolated:

$$w^* = \frac{-c_2 + \sqrt{c_2^2 - 4c_1c_3}}{2c_1} \tag{24}$$

with

$$c_1 = (\rho r_{vap} T - P^*_{vap}) \tag{25}$$

$$c_2 = r_{air} \rho T - P^*_{vap}(1 + \tilde{m}_{vap}/\tilde{m}_{air}) \tag{26}$$

$$c_3 = P^*_{vap} \tilde{m}_{vap}/\tilde{m}_{air} \tag{27}$$

If saturation is reached and the water content in the gas phase decreases, the mixture viscosity evolves accordingly. It is expressed from [20] as follows:

$$\mu = \frac{(1 - \tilde{c}_{vap}) - \mu_{air}}{1 - \tilde{c}_{vap} + \tilde{c}_{vap}\Phi_{av}} + \frac{\tilde{c}_{vap}\mu_{vap}}{\tilde{c}_{vap} + (1 - \tilde{c}_{vap})\Phi_{va}} \tag{28}$$

where

$$\Phi_{av} = \frac{\sqrt{2}}{4}\left(1 + \frac{\tilde{m}_{air}}{\tilde{m}_{vap}}\right)^{-0.5}\left(1 + \left(\frac{\mu_{air}}{\mu_{vap}}\right)^{0.5}\left(\frac{\tilde{m}_{vap}}{\tilde{m}_{air}}\right)^{0.25}\right)^2 \tag{29}$$

$$\Phi_{va} = \frac{\sqrt{2}}{4}\left(1 + \frac{\tilde{m}_{vap}}{\tilde{m}_{air}}\right)^{-0.5}\left(1 + \left(\frac{\mu_{vap}}{\mu_{air}}\right)^{0.5}\left(\frac{\tilde{m}_{air}}{\tilde{m}_{vap}}\right)^{0.25}\right)^2 \tag{30}$$

$\tilde{c}_{vap}$ is the molar concentration of water vapor in the gas phase, related to the humidity ratio as follows:

$$\tilde{c}_{vap} = \frac{1}{1 + \frac{\tilde{m}_{vap}}{w\tilde{m}_{air}}} \tag{31}$$

The deviation from the ideal-gas law and the change of viscosity provide the necessary tools for the modeling of HA-lubricated journal bearings.

3. Numerical computations and results

Journal bearings lubricated with condensable humid air are compared to equivalent non-condensable (ideal gas) cases using two performance metrics, namely the load capacity ratio W_r and the critical mass ratio M_r, defined as follows:

$$W_r = \frac{W_{cond}}{W_{non-cond}} \tag{32}$$

$$M_r = \frac{M_{c,cond}}{M_{c,non-cond}} \tag{33}$$

$$\tag{34}$$

Both the investigated geometries have a L/D ratio of 1. Moreover, the HGJB geometry is based on the design obtained in [21] maximizing the minimum critical mass for the range $\Lambda \in [0, 1]$ (Equation 39) when the grooved member rotates:

$$\alpha = 0.6 \tag{35}$$

$$\hat{\beta} = 145.8^\circ \tag{36}$$

$$H = 2.25 \tag{37}$$

Unless specified differently, the presented simulations are performed at an ambient temperature of 308 K, which is assumed to represent a pessimistic temperature for humid environments. A first simulation of the PJB running at $\Lambda = 30$, and $\epsilon_x = 0.5$ allows to understand the consequences of humid air lubrication. Figure A.3 presents the pressure relative to the ambient at the mid-span of the considered bearing and the relative deviation of the pressure compared to the non-condensable case with an ambient relative humidity of 0.8. The relative humidity ϕ is defined as follows:

$$\phi = \frac{P_{vap}}{P^*_{vap}} \tag{38}$$

The pressure is not only affected in the zone where it exceeds the dew point, exhibiting a reduction larger than 0.8% , but also outside this zone, although the deviation is even more modest. The pressure field is globally affected because of the elliptical characteristic of the Reynolds equation. The pressure value at one particular point affects the entire fluid film domain. This kind of observation is impossible with HA effects considered *a posteriori*, on top of the pressure field computed with non-condensable gas lubrication, as usually seen in the literature [4, 5, 6].

Figure A.4 presents the isolines of the load capacity ratio W_r for the PJB at $\epsilon_x = 0.5$ as a function of the ambient relative humidity ϕ_a and the compressibility number Λ. Load capacity drops when the saturation pressure is reached inside the bearing and the condensation onset is reached at lower values of ϕ_a as Λ increases, until it converges toward a limit value. This is due to the well-known limiting solution for PJB with $\Lambda \to \infty$, at which a limit pressure field is reached. With a maximum relative deviation of approximately 1.5% at this ambient temperature, the loss of load capacity remains low at all values of compressibility number, even at high ambient relative humidity. Deviation of this order of magnitude can be considered as negligible from a practical point of view.

Figure A.5 depicts the evolution of M_r with ϕ_a and Λ. Once the saturation pressure is reached within the gas film, the condensation effects have a small yet negative influence on M_r. Such a modest evolution of the critical mass remains without consequences on the practical design and performance of a PJB.

Figures A.6 and A.7 present the same approach with the HGJB for W_r and M_r respectively, at $\epsilon_x = 0.05$. The load capacity is negatively affected by the condensation, with a maximum deviation of less than 1%. Regarding the stability in the saturated domain, M_r is above unity on the left side of the line $\Lambda \approx 9$ and below unity on its right side. The largest low- and high-deviation values are reached at the line itself, with a very abrupt change of trend. The underlying phenomenon is the point of very high stability observed for HGJB for particular values of Λ. Under the condition of saturated humid air lubrication, the position of this stability peak is shifted to slightly lower values of Λ (Figure A.8), explaining the abrupt variation of M_r in this zone. The divergence of the 25%-deviation lines along the ϕ_a axis translates a rise in the amplitude of this variation with the ambient humidity ratio. However, M_r gets close to 1 as soon as the operating conditions deviate from this particular zone.

From a design perspective, the minimum value of the critical mass between the targeted value of compressibility number Λ^* and 0 bears a particular importance, since it indicates the stability threshold of a bearing accelerating from rest to nominal speed. A new metric is defined to compare the minimum value of the critical mass in this range:

$$M_{r,min} = \frac{\min\limits_{\Lambda \in [0,\Lambda^*]} M_{c,cond}}{\min\limits_{\Lambda \in [0,\Lambda^*]} M_{c,non-cond}} \tag{39}$$

Figure A.9 depicts the evolution of M_r and $M_{r,min}$ with Λ^* for the saturated ambient condition ($\phi_a = 1$). The improvement of critical mass observed for the condensable lubrication on the left-hand side of the turn-over point at $\Lambda^* \approx 9$ is translated into a moderately improved value of the minimum critical mass ($\approx 3\%$). Past this point, $M_{r,min}$ coincides with the line of M_r, resulting in a depreciation of the minimum critical mass reaching 25%, which is not negligible from a design perspective.

The knowledge of the HA-effects on the synchronous stiffness and damping presents a practical interest to predict the imbalance response of a rotor. The total stiffness and damping ratio in the x direction are defined as follows:

$$K_{x,r} = \frac{\left(\sqrt{K_{xx}^2 + K_{yx}^2}\right)_{cond}}{\left(\sqrt{K_{xx}^2 + K_{yx}^2}\right)_{non-cond}} \tag{40}$$

$$C_{x,r} = \frac{\left(\sqrt{C_{xx}^2 + C_{yx}^2}\right)_{cond}}{\left(\sqrt{C_{xx}^2 + C_{yx}^2}\right)_{non-cond}} \tag{41}$$

Figure A.10 presents the synchronous value of these two parameters for the PJB and HGJB as a function of Λ. The stiffness ratio is slightly above 1 for small values of Λ, however without practical significance. The PJB case exhibits a constantly decreasing trend at higher compressibility numbers, converging around a loss lower than 1.5%. The HGJB shows a modest loss of stiffness at intermediate values of Λ and an equally modest gain at low and high values of Λ. However, the deviation remains lower than $\pm 0.5\%$ in all investigated cases, which can be regarded as negligible. Qualitatively, the damping ratio behaves similarly to the stiffness ratio for the PJB, with a rapid decrease and a nearly constant plateau at approximately -2.5% for high values of Λ. The damping ratio of the HGJB exhibits a different trend, as a local minimum at $\Lambda \approx 6$ is visible with a reduction of nearly 3%. At higher compressibility numbers, this parameter increases and exceeds unity with a gain lower than 0.5%. In a practical perspective, the synchronous dynamic coefficients of both bearings can be considered as independent of HA effects.

The effects of the eccentricity ratio on the considered bearings are presented in Figure A.11, at $\Lambda = 10$ and $\phi_a = 0.9$. The evolution of W_r shows no clear trend for the HGJB and diminishes for the PJB as soon as the saturation point is reached, yet in an insignificant order of magnitude. The value of M_r for the HGJB increases slightly because of the further shift in the critical mass curve. The M_r of the PJB shows a local minimum at $\epsilon_x \approx 0.17$, however at levels without practical implications. Both metrics for HGJB are affected by humid-air effects already at a concentric position because of the inherent pressure build-up due to the grooved pattern, while saturation is reached only above $\epsilon_x \approx 0.1$ for the PJB.

Figure A.12 presents the evolution of the minimum value of $M_{r,min}$ for $\Lambda^* = 50$ with the eccentricity ratio, in saturated ambient conditions. This metric shows a minimum at concentric position and relaxes as the eccentricity ratio increases.

The effects of the ambient temperature are presented in Figure A.13 for both PJB and HGJB at $\phi_a = 0.9$. The concentration of water in the gas mixture increases with temperature at equal value of relative humidity, thus enhancing the effects of humid-air lubrication at high ambient temperature. All metrics are affected in significant proportions at temperatures approaching 100 $°C$. The strong enhancement of M_r for the HGJB is due to the fact that the stability peak is shifted to lower values of Λ as the temperature increases with constant ϕ_a. For both bearings, the load capacity is reduced by 2% at a temperature of 330 K. On the same Figure, the minimum value of $M_{r,min}$ for $\Lambda^* = 50$ in saturated ambient conditions is shown in order to represent the worst case scenario. The temperature has a significant influence, since this indicator approaches 0 near 100 $°C$. The humid air effects are still significant on this indicator at lower temperatures, since the 10%-reduction threshold is located at 290 K.

The influence of liquid water droplets formed in the bearing clearance due to condensation can be questioned, since the formation of a liquid phase in the lubrication film can threaten the viability of the bearing. However, because of its significant difference of density at near-normal conditions (three orders of magnitude), the liquid phase, which was neglected in the previous computations, might occupy an insignificant volume in the mixture. In order to analyze this, the void fraction, defined as the volume of gas phase over the total two-phase volume, is used:

$$\delta = \frac{v_{gas}}{v_{liquid} + v_{gas}} \tag{42}$$

Figure A.14 shows the "1-void fraction" of the mixture for different ambient temperature and $\phi_a = 1$ in the situation where all the water from the saturated solution condenses, which is an overestimation of reality. Under this assumption, the void fraction gets the following expression:

$$\delta = \frac{1}{1 + w_a \rho_{air}/\rho_w} \tag{43}$$

The minimum value barely reaches 99% for T just below 100 $°C$, which is suggested to be sufficiently large to discard any risk linked to the formation of a local liquid film in the bearing clearance.

4. Conclusions

A modified form of the Reynolds equation suited for humid-air lubrication was developed and applied to grooved and plain journal bearings on a wide range of operating conditions (compressibility number, eccentricity ratio, ambient temperature and relative humidity). Cases accounting for vapor condensation in the lubrication film were compared to non-condensable cases (ideal gas) in terms of load capacity and stability (critical mass). The investigations lead to the following observations:

- Humid air (HA) lubrication affects the pressure distribution in a lubrication gas film even at locations where the pressure does not exceed the dew pressure

- Consequences of HA lubrication are in general more significant at high compressibility numbers Λ, ambient humidity ratios and eccentricity ratios. High levels of ambient temperature increase the sensitivity of load capacity and stability to humid-air effects, as the mass concentration of water in air increases

- Herringbone-grooved journal bearings (HGJB) are more sensitive to HA effects than plain journal bearings (PJB), notably because of their inherent pressure build-up even at concentric position, whereas PJBs require a higher eccentricity to develop HA effects.

- Vapor condensation negatively affects the load capacity of journal bearings, however without practical significance at temperature levels met in atmospheric conditions ($T_a < 310$ K). The critical mass of PJBs is affected in negligible proportions, while HGJBs can experience a significantly reduced critical mass at particular compressibility numbers, with a reported reduction up to 25% in realistic atmospheric temperatures. In consequence, an equivalent margin is suggested on the critical mass to ensure a safe operation of HGJBs designed from the non-condensable Reynolds equation.

- In realistic situations, the presence of liquid droplets in the bearing clearance is unlikely to be a threat to the integrity of the system due to the very small void fraction calculated in worst-case scenarii.

Acknowledgment

The first author would like to thank Ms.Oïhénart for the provided support. The authors acknowledge the funding by the Swiss National Science Foundation, grant PYAPP2_154278/1.

Reference

[1] D. Zhao, B. Blunier, F. Gao, M. Dou, A. Miraoui, Control of an Ultrahigh-Speed Centrifugal Compressor for the Air Management of Fuel Cell Systems, IEEE Transactions on Industry Applications 50 (3) (2014) 2225–2234. doi:10.1109/TIA.2013.2282838.

[2] Y. Wan, J. Guan, S. Xu, Improved empirical parameters design method for centrifugal compressor in PEM fuel cell vehicle application, International Journal of Hydrogen Energy 42 (8) (2017) 5590–5605. doi:10.1016/j.ijhydene.2016.08.162.

[3] S. Burgmann, T. Fischer, M. Rudersdorf, A. Roos, A. Heinzel, J. Seume, Development of a centrifugal fan with increased part-load efficiency for fuel cell applications, Renewable Energy 116 (2018) 815–826. doi:10.1016/j.renene.2017.09.075.

[4] B. Strom, Shuyu Zhang, Sung Chang Lee, A. Khurshudov, G. Tyndall, Effects of Humid Air on Air-Bearing Flying Height, IEEE Transactions on Magnetics 43 (7) (2007) 3301–3304. doi:10.1109/TMAG.2007.897085.

[5] S. Zhang, B. Strom, S.-C. Lee, G. Tyndall, Simulating the Air Bearing Pressure and Flying Height in a Humid Environment, Journal of Tribology 130 (1) (2008) 011008. doi:10.1115/1.2805424.

[6] W. Hua, W. Zhou, B. Liu, S. Yu, C. H. Wong, Effect of environment humidity and temperature on stationary and transient flying responses of air bearing slider, Tribology International 42 (8) (2009) 1125–1131. doi:10.1016/j.triboint.2008.09.010.

[7] S. Kirpekar, O. Ruiz, Computing the performance of an air bearing in humid conditions, Applied Physics Letters 94 (23) (2009) 234103. doi:10.1063/1.3139757.

[8] Y. Ma, B. Liu, Contribution of water vapor to slider air-bearing pressure in hard disk drives, Applied Physics Letters 90 (22) (2007) 223502. doi:10.1063/1.2743745.

[9] Y. Ma, B. Liu, Further Study of the Effect of Water Vapor on Slider Air Bearing, IEEE Transactions on Magnetics 45 (11) (2009) 5006–5009. doi:10.1109/TMAG.2009.2029421.

[10] Y. Aoki, K. Takahashi, J. Li, J. Xu, Y. Ooeda, Humidity effect on head-disk clearance, Microsystem Technologies 17 (5-7) (2011) 1051–1056. doi:10.1007/s00542-011-1291-1.

[11] J. Choi, N.-C. Park, Y.-P. Park, K.-S. Park, E.-J. Hong, Y. Lee, C.-S. Kim, Analysis of Thermal Flying-Height Control System About Humid Air Condition in Hard Disk Drive, in: ASME 2014 Conference on Information Storage and Processing Systems, 2014, p. V001T01A015. doi:10.1115/ISPS2014-6958.

[12] H. Tani, J. Tomita, S. Koganezawa, N. Tagawa, Effect of Vapor Lubrication on HeadDisk Clearance and Slider Wear in Inert Gas Environments, in: ASME 2014 Conference on Information Storage and Processing Systems, 2014, p. V001T01A007. doi:10.1115/ISPS2014-6931.

[13] Y. S. Ma, W. D. Zhou, S. K. Yu, W. Hua, Adsorbed Water Film and Heat Conduction from Disk to Slider in Heat-Assisted Magnetic Recording, Tribology Letters 56 (1) (2014) 93–99. doi:10.1007/s11249-014-0388-y.

[14] L. M. Matthes, R. Brunner, B. Knigge, F. E. Talke, Head Wear of Thermal Flying Height Control Sliders as a Function of Bonded Lubricant Ratio, Temperature, and Relative Humidity, Tribology Letters 60 (3) (2015) 39. doi:10.1007/s11249-015-0614-2.

[15] L. M. Matthes, F. E. Spada, A. Ovcharenko, B. E. Knigge, F. E. Talke, Effect of HeadDisk Interface Biasing and Relative Humidity on Wear of Thermal Flying Height Control Sliders, Tribology Letters 65 (2) (2017) 44. doi:10.1007/s11249-017-0828-6.

[16] J. W. Lund, Calculation of Stiffness and Damping Properties of Gas Bearings, Journal of Lubrication Technology 90 (4) (1968) 793–803. doi:10.1115/1.3601723.

[17] E. Guenat, J. Schiffmann, Real-gas effects on aerodynamic bearings, Tribology International 120 (2018) 358–368. doi:10.1016/j.triboint.2018.01.008.

[18] J. H. Vohr, C. Y. Chow, Characteristics of Herringbone-Grooved, Gas-Lubricated Journal Bearings, Journal of Basic Engineering 87 (3) (1965) 568–576. doi:10.1115/1.3650607.

[19] I. H. Bell, J. Wronski, S. Quoilin, V. Lemort, Pure and Pseudo-pure Fluid Thermophysical Property Evaluation and the Open-Source Thermophysical Property Library CoolProp, Industrial & Engineering Chemistry Research 53 (6) (2014) 2498–2508. doi:10.1021/ie4033999.

[20] P. Tsilingiris, Thermophysical and transport properties of humid air at temperature range between 0 and 100C, Energy Conversion and Management 49 (5) (2008) 1098–1110. doi:10.1016/j.enconman.2007.09.015.

[21] D. P. H. Fleming, Optimization of self-acting herringbone journal bearings for maximum stability, in: 5th International Gas Bearing Symposium, 1974.

Appendix A. NGT

The terms composing equation 16 are developed here.

$$\bar{h}_r = \frac{h_r}{h_0} = \frac{h_r}{h_r(\epsilon = 0)} \tag{A.1}$$

$$\bar{h}_g = \frac{h_g}{h_0} \tag{A.2}$$

$$H = \frac{h_g(\epsilon = 0)}{h_0} \tag{A.3}$$

$$g_1 = \bar{h}_g^3 \bar{h}_r^3 \tag{A.4}$$

$$g_2 = (\bar{h}_g^3 - \bar{h}_r^3)^2 \alpha(1 - \alpha) \tag{A.5}$$

$$g_3 = (1 - \alpha)\bar{h}_g^3 + \alpha \bar{h}_r^3 \tag{A.6}$$

$$c_s = -\frac{6\mu\Omega R^2}{p_a h_0^2} \alpha(1 - \alpha)(H - 1)\sin\hat{\beta} \tag{A.7}$$

$$f_1 = \frac{g_1 + g_2 \sin^2 \hat{\beta}}{g_3} \tag{A.8}$$

$$f_2 = \frac{g_2 \sin\hat{\beta}\cos\hat{\beta}}{g_3} \tag{A.9}$$

$$f_3 = \frac{g_1 + g_2 \cos^2 \hat{\beta}}{g_3} \tag{A.10}$$

$$f_4 = \frac{\bar{h}_g^3 - \bar{h}_r^3}{g_3} \tag{A.11}$$

$$f_5 = \alpha \bar{h}_g + (1 - \alpha)\bar{h}_r \tag{A.12}$$

List of Figures

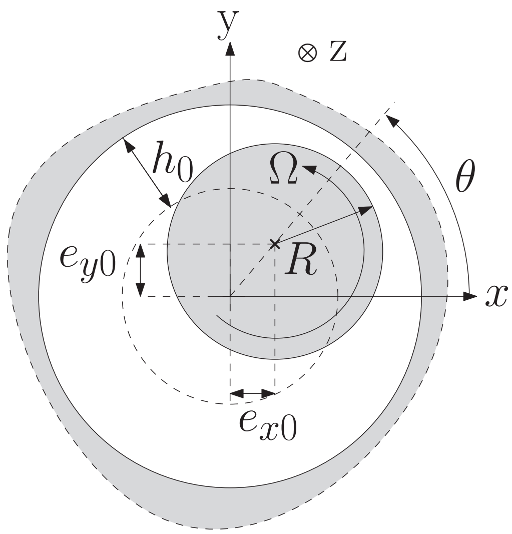

Figure A.1: Nomenclature of a journal bearing

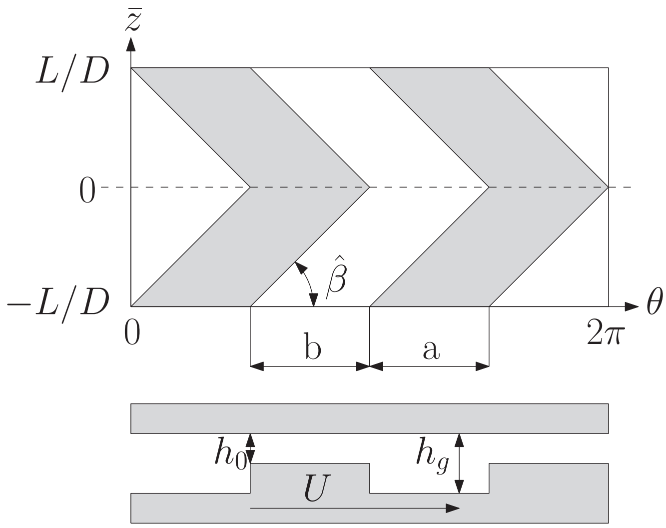

Figure A.2: Geometry and nomenclature of a HGJB

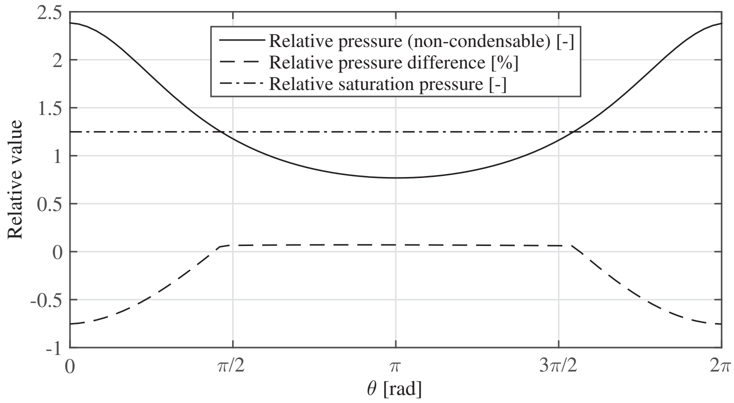

Figure A.3: Relative pressure and deviation along the circonference of a PJB at $\bar{z} = 0$, $\epsilon_x = 0.5$, $\phi_a = 0.8$ and $\Lambda = 30$)

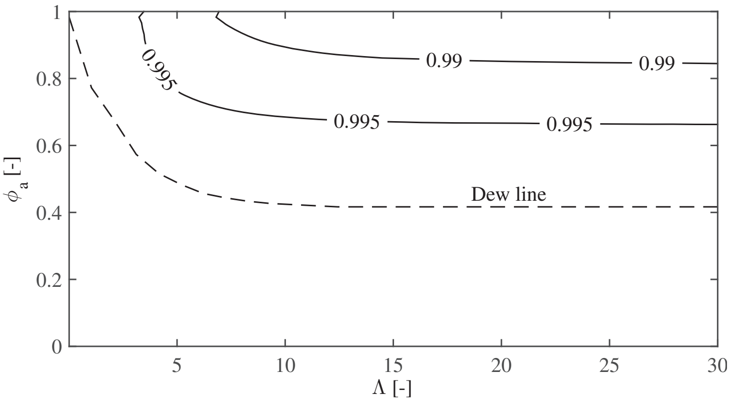

Figure A.4: Isolines of W_r for PJB at $\epsilon_x = 0.5$ ($T_a = 308$ K)

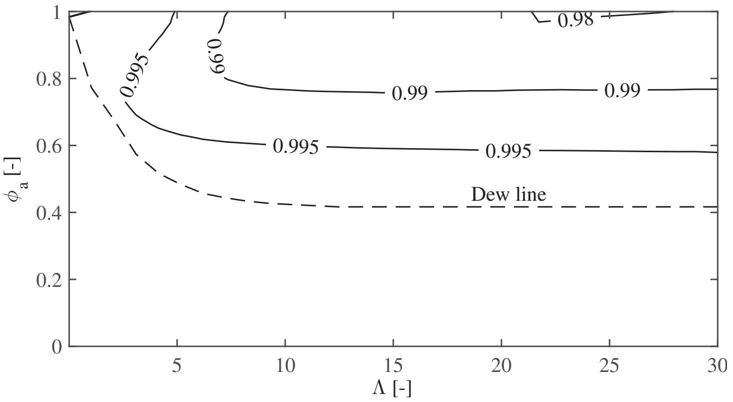

Figure A.5: Isolines of M_r for PJB at $\epsilon_x = 0.5$ ($T_a = 308$ K)

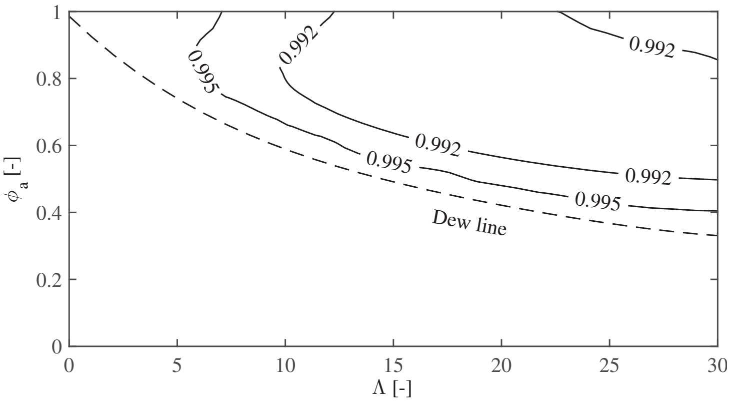

Figure A.6: Isolines of W_r for HGJB at $\epsilon_x = 0.05$ ($T_a = 308$ K)

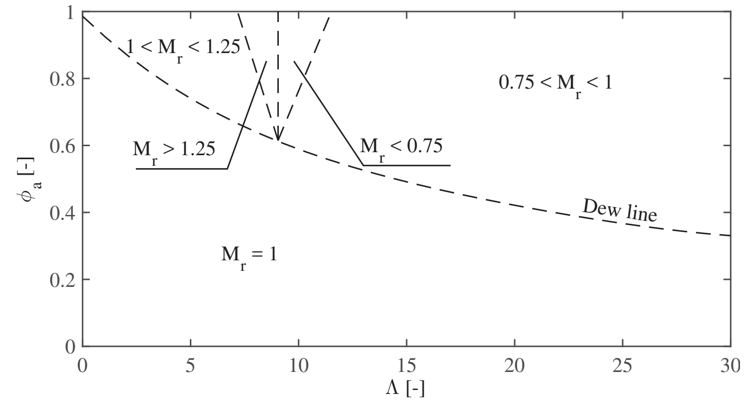

Figure A.7: Isolines of M_r for HGJB at $\epsilon_x = 0.05$ ($T_a = 308$ K)

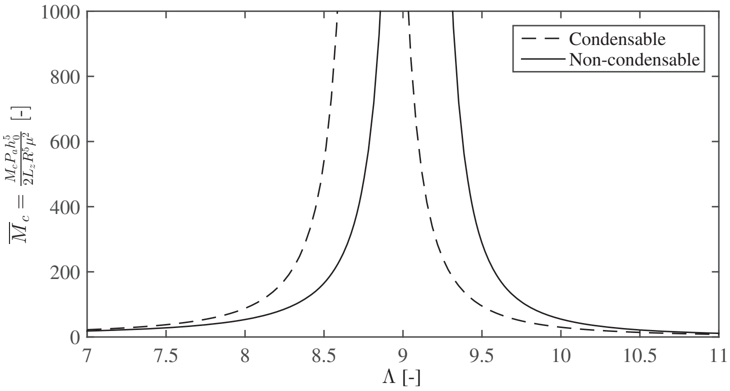

Figure A.8: Critical mass for HGJB at $\epsilon_x = 0.05$ ($T_a = 308$ K, $\phi_a = 1$) as a function of Λ with and without vapor condensation

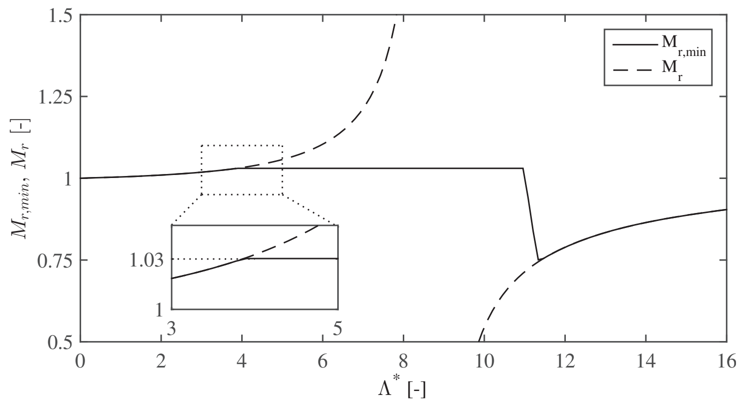

Figure A.9: M_r and $M_{r,min}$ for HGJB at $\epsilon_x = 0.05$ ($T_a = 308$ K, $\phi_a = 1$) as a function of Λ

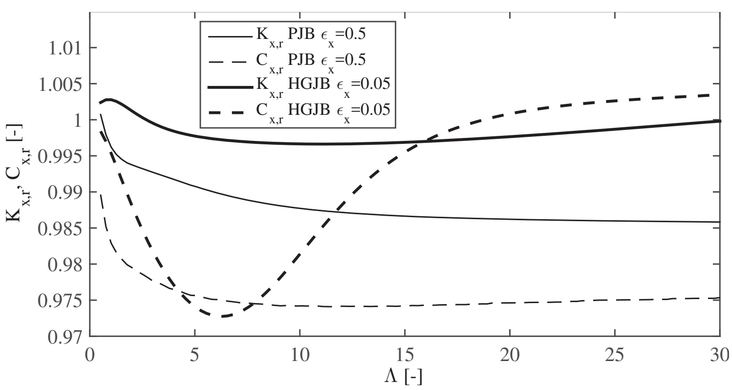

Figure A.10: Evolution of total stiffness and damping ratio for PJB and HGJB ($T_a = 308$ K, $\phi_a = 1$) as a function of Λ

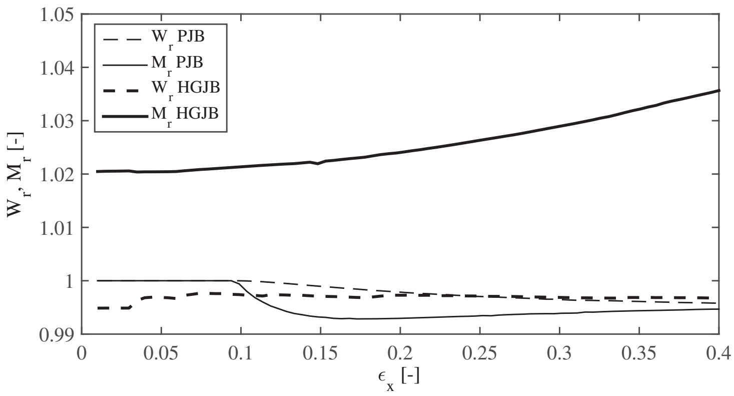

Figure A.11: Evolution of W_r and M_r for HGJB and PJB with the eccentricity ratio (T_a= 308 K. Λ=5, ϕ_a=0.9)

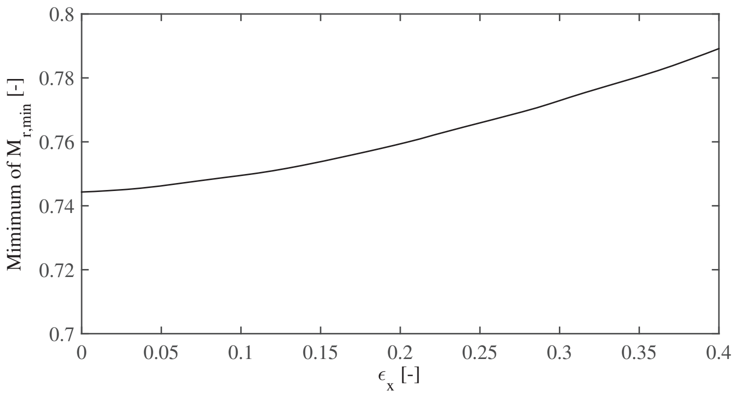

Figure A.12: Evolution of the minimum value of $M_{r,min}$ for $\Lambda^* = 50$ with the eccentricity ratio for HGJB (T_a= 308 K, ϕ_a=1)

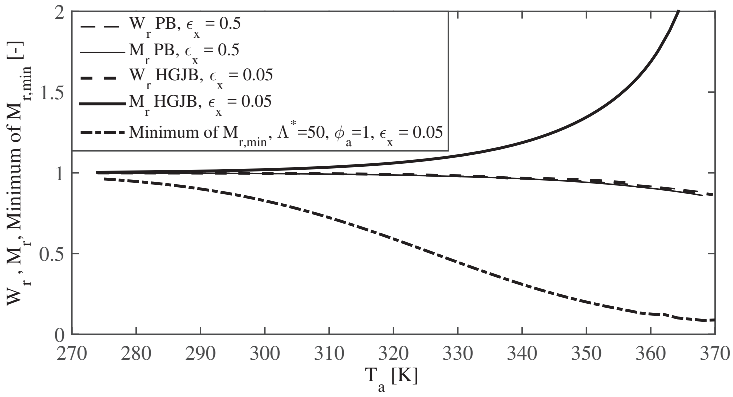

Figure A.13: Evolution of W_r and M_r for HGJB and PJB with the ambient temperature ($\Lambda = 5$, ϕ_a=0.9), together with the evolution of the minimum value of $M_{r,min}$ for ϕ_a=1

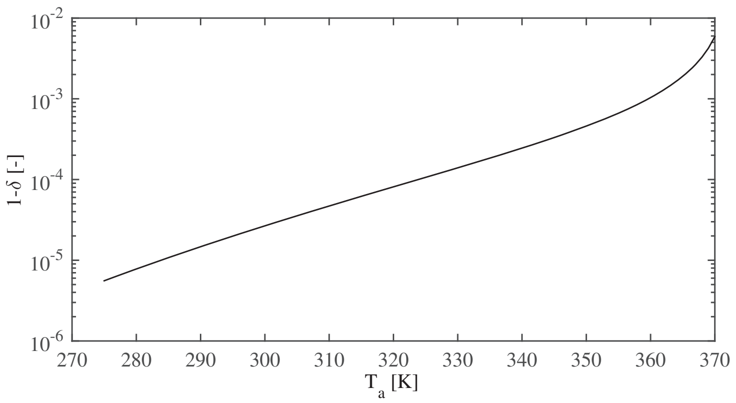

Figure A.14: Void fraction as a function of temperature in the limit case where all the water content condenses (ϕ_a=1)